Solid-state formation of CO 2 via the H 2 CO + O reaction

M. Minissale, J.-C. Loison, S. Baouche, H. Chaabouni, E. Congiu, F. Dulieu

A&A 577, A2 (2015)
DOI: 10.1051/0004-6361/201424342

Astronomy & Astrophysics

Solid-state formation of CO_2 via the H_2CO + O reaction⋆

M. Minissale[1,2,3], J.-C. Loison[4], S. Baouche[1,2,3], H. Chaabouni[1,2,3], E. Congiu[1,2,3], and F. Dulieu[1,2,3]

[1] Université de Cergy Pontoise, UMR 8112, LERMA, 95000 Cergy Pontoise Cedex, France
[2] LERMA, Observatoire de Paris, PSL Research University, CNRS, UMR 8112, 75014 Paris, France
e-mail: marco.minissale@obspm.fr
[3] Sorbonne Universités, UPMC Univ. Paris 6, UMR 8112, LERMA, 75005 Paris, France
[4] ISM – Université de Bordeaux – CNRS, UMR 5255, 351 cours de la Libération, 33405 Talence Cedex, France

Received 5 June 2014 / Accepted 15 December 2014

ABSTRACT

Context. The formation of carbon dioxide ice in quiescent regions of molecular clouds has not yet been fully understood, even though CO_2 is one the most abundant species in interstellar ices.
Aims. CO_2 formation was studied via oxidation of formaldehyde molecules on cold surfaces under conditions close to those encountered in quiescent molecular clouds to evaluate the efficiency and the activation barrier of the H_2CO + O reaction.
Methods. Formaldehyde ices were exposed to O atoms using a differentially pumped beam line. The H_2CO + O reaction experiments were carried out on two different surfaces of astrophysical interest (amorphous water ice and oxidised graphite) held at 10 or 55 K. The products were probed via infrared and mass spectroscopy by using RAIRS and temperature-programmed desorption techniques.
Results. In this paper we show that the H_2CO + O reaction can efficiently form carbon dioxide in the solid phase. The activation barrier for the reaction, based on a model fit to the experimental data, was estimated to be 335 ± 55 K.
Conclusions. The H_2CO+O reaction on cold surfaces can be added to the set of pathways that lead to carbon dioxide in the interstellar ices. Astrophysically, the abundance of CO_2 in quiescent molecular clouds may potentially be explained by three reactions occurring on cosmic grains: CO + OH, CO + O, and H_2CO + O.

Key words. astrochemistry – atomic processes – ISM: atoms – ISM: clouds – ISM: molecules – molecular processes

1. Introduction

Formaldehyde (H_2CO) was the first polyatomic organic molecule detected in the interstellar medium (ISM; Zuckerman et al. 1970). It was detected through the $1_{11}-1_{10}$ ground-state rotational transition at 4830 MHz (Snyder et al. 1969), and its distribution was found to be similar to HII and CO in different environments, such as our Galaxy (Davies & Few 1979; Tang et al. 2013, and references therein), and in Galactic radio sources (Downes et al. 1980).

H_2CO has been observed in some comets (Crovisier & Bockeleé-Morvan 1999; Mumma et al. 2005) and in interstellar ices (Keane et al. 2001). Its abundance with respect to water ice varies from 1% to 6% in high (Keane et al. 2001; Dartois 2005) or low (Boogert et al. 2008) mass protostars, or hot corinos (Maret et al. 2004). Gas-phase reactions (Shalabiea & Greenberg 1994) and UV photolysis of H_2O-CO ice (Allamandola et al. 1988; Schutte et al. 1996; Watanabe et al. 2007) can efficiently produce formaldehyde, but surface reactions, such as hydrogenation of CO ice (studied experimentally by Hiraoka et al. 1994, Watanabe & Kouchi 2002, and Madzunkov et al. 2009, and theoretically by Rimola et al. 2014) are needed to explain the observed abundance of H_2CO in the solid phase.

Formaldehyde is a key species for the grain-surface chemistry of interstellar clouds (Schutte et al. 1993a,b). Hidaka et al. (2004) and Fuchs et al. (2009) show that formaldehyde can form methanol (CH_3OH) through H-atom additions or produce CO via H-atom abstractions. Moreover, H_2CO is involved in the formation of large molecules containing C-H, C-O, O-H, and C-N bonds (Schutte et al. 1993b). During the warm-up of the ice on grains, formaldheyde can react with NH_3, H_2O, and itself (H_2CO) to form amines, diols, or [-CH_2-O-]$_n$ groups (Noble et al. 2012b; Theulé et al. 2013; Mispelaer et al. 2013); for this reason, it could be considered a primary precursor of some complex organic materials (Schutte et al. 1993b). In this paper, we present an experimental study showing that formaldehyde reacts with ground-state O(^{3}P) atoms to form CO_2, one of the most abundant species of interstellar ices. Formaldehyde seems to play a crucial role in the chemistry of interstellar ices and, in particular, in the balance between CO_2, CH_3OH, and CO.

This paper is organised as follows. The experimental setup and methods are described in the next section. In Sect. 3, we present our experimental results showing how H_2CO is consumed by O to form CO_2. In Sect. 4, we present a rate equation model that simulates our results and gives relevant energetic parameters, and we discuss the solid-state network by presenting DFT calculations. In the last section, we discuss the main conclusions and astrophysical implications of this study.

2. Experimental

The experiments were conducted with the FORMOLISM (FORmation of MOLecules in the InterStellar Medium) set-up described extensively elsewhere (Amiaud et al. 2006; Congiu et al. 2012). It consists of a UHV main chamber with a base pressure of 10^{-10}–10^{-11} mbar and two triply differentially pumped atom lines. The ultra-high vacuum chamber contains an oxidised slab of high-oriented pyrolytic graphite (HOPG, 0.9 cm in diameter), operating at temperatures between 8 K and 400 K. The temperature is controlled by a calibrated silicon-diode sensor and a thermocouple (AuFe/Chromel K-type) clamped on

⋆ Appendices are available in electronic form at http://www.aanda.org

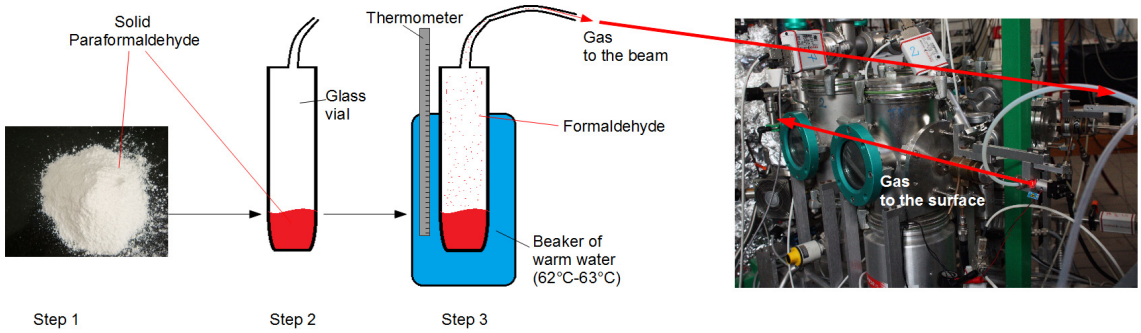

Fig. 1. Detail of the experimental set-up and scheme of the depolymerization process of paraformaldehyde and preparation of the formaldehyde beam.

Table 1. Ion count per second of masses 30, 29, 28, and 18 a.m.u. as a function of pumping time of the paraformaldehyede powder held at 62 °C.

Pumping time (min)	H_2CO Mass 30	H_2CO Mass 29	H_2O Mass 18	CO Mass 28	$\frac{H_2O}{H_2CO}$ [a]	$\frac{CO}{H_2CO}$ [a]
	Signal$_{(Flag\,Open-Flag\,Closed)}$ [b] (cps)				%	
0	580	420	920	1300	92	130
10	650	490	520	1100	45	96
25	740	570	150	620	11	47
50	810	680	10	140	1	9
90	810	690	0	150	0	10

Notes. These signals correspond to the detection of H_2CO (mass 30 and 29), CO (mass 28), and H_2O (mass 18). [(a)] These values indicate the percentage of H_2O and CO with respect to H_2CO. The values were obtained through the formulae 100*Mass18/(Mass29+Mass30) and 100*Mass28/(Mass29+Mass30) for H_2O and CO, respectively. [(b)] Difference between the signal recorded with the flag open and with the flag closed .

the sample holder. Adsorbates and products were probed in situ through Fourier Transform Reflection Absorption InfraRed Spectroscopy (FT-RAIRS) and a quadrupole mass spectrometer (QMS) used for measuring the beam flux and beam composition and for performing the temperature-programmed desorption (TPD) experiments. Amorphous solid water (ASW) ice was grown on the graphite sample, maintained at 120 K, through a leak valve positioned at 2 cm far from the surface.

All the experiments were performed by sending O atoms on formaldehyde ice films previously grown on the cold sample. The two species were deposited by using the same beam line at different times. Figure 1 shows how gaseous formaldehyde is obtained: paraformaldehyde (a white crystalline powder) contained in a pyrex phial is depolymerizated by immersion in a bath at 62 °C. The products of the depolymerization process are H_2CO, CO, and H_2O. Table 1 shows the resulting beam composition measured with QMS (direct beam) at a source pressure of 0.42 mbar as a function of the pumping time. In particular, we report the difference between the signal recorded with the flag[1] open and the signal recorded with the flag closed to account for noise signals.

As shown in Table 1, the ratio between these species varies during the depolymerization process: at the beginning the H_2O/H_2CO ratio is 920/(Mass30+Mass29) ≈ 0.92 and becomes 0 after 90 min of pumping. This means that the sublimation process of paraformaldehyde is able to purify the sample by eliminating the residual H_2O. Similar behaviour concerns the CO/H_2CO ratio, which goes from 1.3 to 0.1; in this case, the resulting gas contains some residual CO even after 90 min of pumping. For this reason, formaldehyde ice films were grown at temperatures higher than those of CO desorption (>55 K). As we discuss in Sect. 3 and Appendix A, we used different isotopologues of formaldehyde to constrain our findings better, i.e., $H_2^{12}CO$, $D_2^{12}CO$, and $H_2^{13}CO$. In the case of $D_2^{12}CO$, the purity is of about 98%, while for $H_2^{13}CO$ is of 99%. Hereafter we refer to ^{12}C simply as C.

Oxygen atoms are generated by (in the ^3P ground state) dissociating O_2 molecules in a quartz tube placed within a Surfatron cavity, which can deliver a maximum microwave power of 200 W at 2.45 GHz (Minissale et al. 2014). We studied the electronic state composition of oxygen beam by tuning the energy of the ionizing electrons of the QMS. This technique allows ground state or electronic excited atoms and molecules to be selectively detected, as described in Congiu et al. (2009). We find that our source is free of $O(^1D)$ and $O_2(a^1\Delta_g^-)$ and is composed only of $O(^3P)$ and $O_2(X^3\Sigma_g^-)$ (see details in Minissale 2014 and Minissale et al. 2014).

With the microwave source turned on, the dissociation efficiency of O_2 was $\tau = 70 \pm 5\%$, where τ represents the percentage of dissociated O_2 molecules and τ is proportional to the microwave power used, so it also defines the O/O_2 ratio in the beamline. If τ is 0.7, every ten O_2 molecules, we will have 14 O atoms and 3 O_2 undissociated molecules. Atoms and undissociated molecules are cooled and instantaneously thermalised upon surface impact with the walls of the quartz tube.

We calibrated the molecular beam as described in Amiaud et al. (2007) and Noble et al. (2012). The first monolayer (1 ML = 10^{15} molecules cm^{-2}) of formaldehyde was reached after an exposure time of about 12 min, and 1 ML of O_2 was reached after six minutes, which give a flux of $\phi_{H_2CO} = (1.3 \pm 0.4) \times 10^{12}$ and $\phi_{O_2off} = (3.0 \pm 0.3) \times 10^{12}$ molecules cm^{-2} s^{-1}, respectively. Once the O_2 discharge is turned on, the O-atom flux is $\phi_O = 2\tau\phi_{O_2off} = 5.4 \times 10^{12}$ atoms cm^{-2} s^{-1} and the O_2 flux $\phi_{O_2on} = (1 - \tau)\,\phi_{O_2off} = 10^{12}$ molecules cm^{-2} s^{-1}.

[1] The flag is a rotatable metallic plate used to provisionally isolate the beam line from the main chamber.

Table 2. List of experiments.

Experiment	Thickness (ML)	R_{dep} (L/min)	T_{dep} (K)	$T_{atom-add}$ (K)	Atom-fluence (10^{16} atoms/cm^2)	t (min)
		$H_2^{12}CO$, O_2 on graphite			(O from O_2)	
$H_2^{12}CO$+O:O_2	2	0.12, 0.035	60	10	0.5	24
$H_2^{12}CO$	2	0.12, 0.035	60	–	–	–
O:O_2	2	0.12, 0.035	–	10	0.5	24
$H_2^{12}CO$+O:O_2	2	0.12, 0.035	60	55	0.7	30
		H_2O, $H_2^{12}CO$, O_2				
H_2O+$H_2^{12}CO$+O:O_2	50:2	2.4, 0.08, 0.02	60	10	0.5	24
H_2O+$H_2^{12}CO$+O:O_2	50:2	2.4, 0.08, 0.02	60	55	0.7	30
H_2O+$H_2^{12}CO$	50:2	2.4, 0.08, 0.02	60	–	–	–
		$H_2^{13}CO$, O_2 on graphite				
$H_2^{13}CO$+O:O_2	2	0.12, 0.035	60	55	0.5	24
$H_2^{13}CO$	2	0.12, 0.035	60	–	–	–
O:O_2	2	0.12, 0.035	–	10	0.5	24
		$D_2^{12}CO$, O_2 on graphite				
$D_2^{12}CO$+O:O_2	2	0.12, 0.035	60	55	0.5	24
$D_2^{12}CO$	2	0.12, 0.035	60	–	–	–
		$H_2^{12}CO$, O_2 on graphite				
$H_2^{12}CO$+O_2	1.5:1.5	0.12, 0.035	60, 15	–	–	–
		$H_2^{12}CO$, O_3 on graphite				
$H_2^{12}CO$+O_3	1.5:1.5	0.12, 0.035	60	–	–	–

Notes. The + and : signs indicate sequential deposition and codeposition, respectively. The thickness is expressed in monolayers (ML); R_{dep} is the deposition rate of a selected molecule expressed in Langmuir (L) min^{-1}, where 1 L = 1.3 × 10^{-6} mbar s^{-1}; T_{dep} is the substrate temperature during deposition; $T_{atom-add}$ is the substrate temperature during O-atom addition; atom-fluence is the total fluence at the end of the experiment; t is the time of atom addition.

CO_2 formation was investigated on two different surfaces, ASW and an oxidised slab of HOPG. In Table 2 we display a complete list of experiments providing details on the species and dose of the reactive molecule deposited. Different doses of O (+O_2) were sent onto formaldehyde ice. (The coverage of H_2CO ices was always <2.5 ML.) During each phase (ices growth or O-atom deposition), the surface was held at a given constant temperature. After each O-atom deposition, the products were probed using RAIR spectroscopy. After about 5 ML of oxygen, atoms were deposited, and the surface was heated with a linear temperature ramp of 10 K/min, until the adsorbates had fully desorbed from the surface (around 200 K). For each substrate (ASW ice or graphite), we adopted two deposition temperatures (10 and 60 K). We also performed experiments to determine whether CO_2 was formed via H_2CO + O_2 and H_2CO + O_3. For this purpose, we performed two sets of TPD experiments. First, the H_2CO+O_2 reaction was checked by depositing 2 ML of O_2 on top of H_2CO films. The H_2CO+O_3 reaction was studied through a similar experiment except that H_2CO was deposited on top of O_3. In fact, for technical reasons, we had previously produced ozone via the O+O_2 reaction on the surface at 10 K, eliminated the residual O_2 by heating the surface to 50 K, and only then deposited H_2CO at 60 K.

3. Experimental results

3.1. Oxygenation of H_2CO ices

In this section we present the experimental results showing the products of the reactions H_2CO + O_x (O, O_2, and O_3). The oxygen beam that we used to irradiate formaldehyde also contains O_2 molecules, therefore O_3 can be formed on the surface at temperatures lower than <55 K (Minissale et al. 2014).

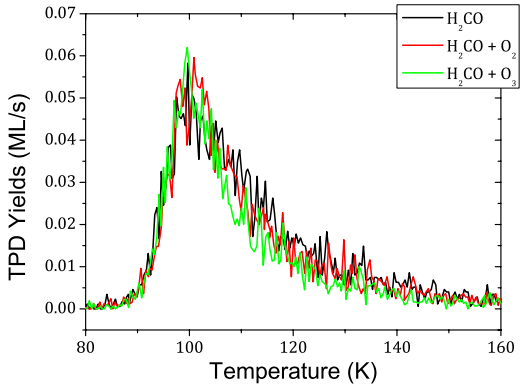

Fig. 2. H_2CO TPD traces obtained after deposition of 1 ML of H_2CO (black line), H_2CO+O_2 (red line), and H_2CO+O_3 (green line) on oxidised HOPG held at 10 K.

For this reason, we first studied the reactions H_2CO + O_2/O_3, then the reaction H_2CO + O. Figure 2 shows three TPD spectra of mass 30 a.m.u. (H_2CO) after depositing 1 ML of H_2CO, 1 ML of H_2CO+O_2, and 1 ML of H_2CO+O_3 on oxidised HOPG held at 10 K . The three TPD curves and their integrated areas are very similar, suggesting that H_2CO has not been consumed by O_2 or O_3.

Actually, this is not a surprising result since the reactions

$$H_2CO + O_2 \rightarrow HCO + HO_2 \ (\Delta H = +160 \text{ kJ/mol}) \quad (1)$$

$$H_2CO + O_3 \rightarrow HO_2 + HCO_2 \ (\Delta H > 200 \text{ kJ/mol}) \quad (2)$$

are endothermic[2] and present high (>1600 K/k_b) activation barriers (Michael et al. 1999; Braslavsky & Heicklen 1976).

[2] NIST Chemistry WebBook.

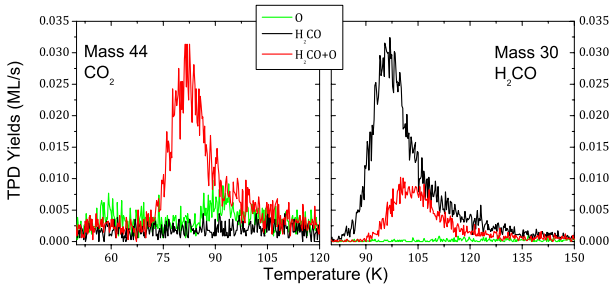

Fig. 3. CO_2 (*left panel*) and H_2CO (*right panel*) TPD traces obtained after deposition of 2 ML of H_2CO (black line), 5 ML of O (green line), and 2 ML of H_2CO + 5 ML of O atoms (red line) on oxidised HOPG held at 10 K.

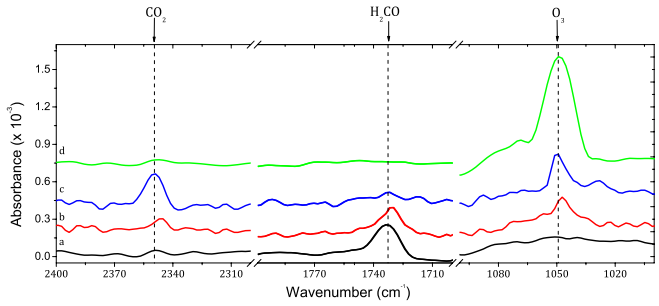

Fig. 4. Four RAIR spectra obtained after deposition of (a) 2 ± 0.5 ML of H_2CO; (b) 2±0.5 ML of H_2CO+0.8±0.1 ML of O atoms; (c) 2±0.5 ML of H_2CO+5±0.4 ML of O atoms; (d) 5±0.4 ML of O atoms on oxidised HOPG held at 10 K. (H_2CO was always deposited at 60 K.)

Moreover, the inefficiency of reactions (1) and (2) is confirmed by the absence of newly formed species.

Figure 3 shows the TPD curves of CO_2 (mass 44, left panel) and H_2CO (mass 30, right panel) for three different sequential deposition experiments on oxidised HOPG held at 10 K: 2 ± 0.5 ML of H_2CO, 2 ± 0.5 ML of H_2CO + 5 ± 0.3 ML of O atoms alone, and 5 ± 0.3 ML of O atoms.

The green line represents a control experiment carried out to be certain that CO_2 is not present in the O beam and that carbon dioxide was actually formed on the surface because of H_2CO oxygenation. In fact, a signal at mass 44 (CO_2) is visible in Fig. 3 (left panel) and could come either from the O beam or from oxygenation of residual CO. In either case, it is ten times weaker than the mass-44 signal coming from H_2CO oxygenation experiment (left panel of Fig. 3). For this reason, it is fair to believe that H_2CO ice is consumed upon oxygen irradiation (right panel) and that CO_2 is formed.

Further evidence of H_2CO consumption and CO_2 formation is provided by the RAIR spectra shown in Fig. 4. Curve a in Fig. 4 shows the RAIR spectrum after deposition of 2 ML of H_2CO on an oxidised HOPG held at 60 K to avoid CO adsorption. We assign the band at 1732 cm^{-1} to the CO stretch of H_2CO. H_2CO was then exposed to increasing doses of O atoms. Curves b and c in Fig. 4 show the cases of 2 ML H_2CO+0.8±0.1 and 5 ± 0.4 ML of O atoms. Here two new bands are visible: the first one, peaking between 2349–2345 cm^{-1}, is assigned to the anti symmetric stretch of CO_2. The second band, peaking at 1047 cm^{-1}, is due to the ν_3 asymmetric stretching mode of O_3 and is also present in spectrum d, where O atoms were deposited on the bare surface. All the IR bands of interest for this paper are listed in Table 3.

We obtained similar results when the experiments were performed on ASW ices. Figure 5 shows RAIR spectra recorded

Table 3. List of infrared features in the RAIR spectra shown in Figs. 4–6, and A.1.

Molecule	Mode	Wavenumber (cm^{-1})
$H_2^{12}CO$	CO str	1733 ± 1[a]
	CH_2 scis	1502 ± 1
	CH_2 rock	1247 ± 2
$H_2^{13}CO$	^{13}CO str	1697
	$^{13}CH_2$ scis	1502
	$^{13}CH_2$ rock	1174
$D_2^{12}CO$	CO str	1680
	CD_2 a-scis	2154
O_3	O-O a-str	1047–1042[b]
$^{12}CO_2$	Anti str	2347 ± 2–2359[b]
$^{13}CO_2$	Anti str	2285

Notes. [(a)] "±" considers the small shifts of the IR features during the same set of measurements ;[(b)] the two values refer to features in spectra obtained after O-atom irradiation of $H_2^{12}CO$ and $D_2^{12}CO$, respectively.

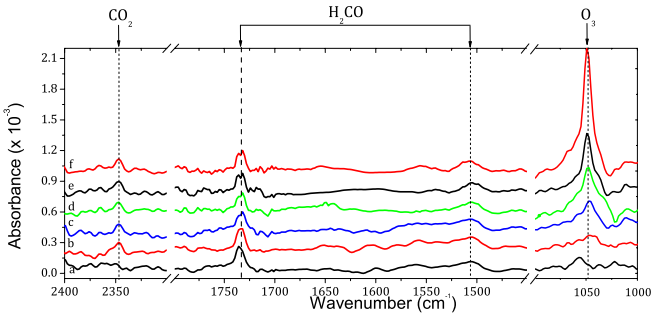

Fig. 5. Six RAIR spectra obtained after deposition of (a) 2 ± 0.5 ML of H_2CO; (b) 2 ± 0.5 ML of H_2CO + 0.5 ± 0.1 ML of O atoms; (c) 2 ± 0.5 ML of H_2CO + 0.8 ± 0.1 ML of O atoms; (d) 2 ± 0.5 ML of H_2CO + 1.2 ± 0.2 ML of O atoms; (e) 2 ± 0.5 ML of H_2CO + 2.0 ± 0.3 ML of O atoms; (f) 2 ± 0.5 ML of H_2CO + 3.8 ± 0.3 ML of O atoms, on a ASW ice held at 10 K. (H_2CO was always deposited at 60 K.)

after irradiation at 10 K, of 2 ± 0.5 ML of H_2CO with increasing doses of oxygen atoms (0, 0.5, 0.8, 1.2, 2, 3.8 ML from curves a to f, respectively). As in the previous case, three main spectral features are visible: at 1048 cm^{-1} due to O_3, at 1734 cm^{-1} due to the CO stretch of H_2CO, and finally at 2347 cm^{-1} where the antisymmetric stretch of CO_2 appeared. Also, we assign the weak and broad band at 1502 cm^{-1} to the CH_2 scissoring of H_2CO.

The different substrates (HOPG or compact ASW ice) are responsible for small shifts in the IR features, as well as for a change in the band intensities. Actually, under the same conditions (equal amount of O sent onto H_2CO), HOPG facilitates CO_2 formation slowing down that of O_3, while the ASW substrate favours O_3 formation. This is a consequence of two effects:

- different diffusion constants of O atoms on oxidised HOPG and on ASW ice, i.e., $k_{\mathrm{diff-HOPG}} < k_{\mathrm{diff-ASW}}$ (Congiu et al. 2014);
- different probabilities of chemical desorption for O_2, i.e., $\epsilon_{\mathrm{diff-HOPG}} > \epsilon_{\mathrm{diff-ASW}}$ (Dulieu et al. 2013; Minissale & Dulieu 2014).

Fast diffusion of O atoms and the low probability of chemical desorption of O_2 on ASW allow O atoms to allotropize into O_2 and into O_3 ($[O_3] \gg [CO_2]$). Conversely, on HOPG, the surface density of O_2 decreases due to chemical desorption. The O atoms stay on the surface longer, have a higher probability of reacting

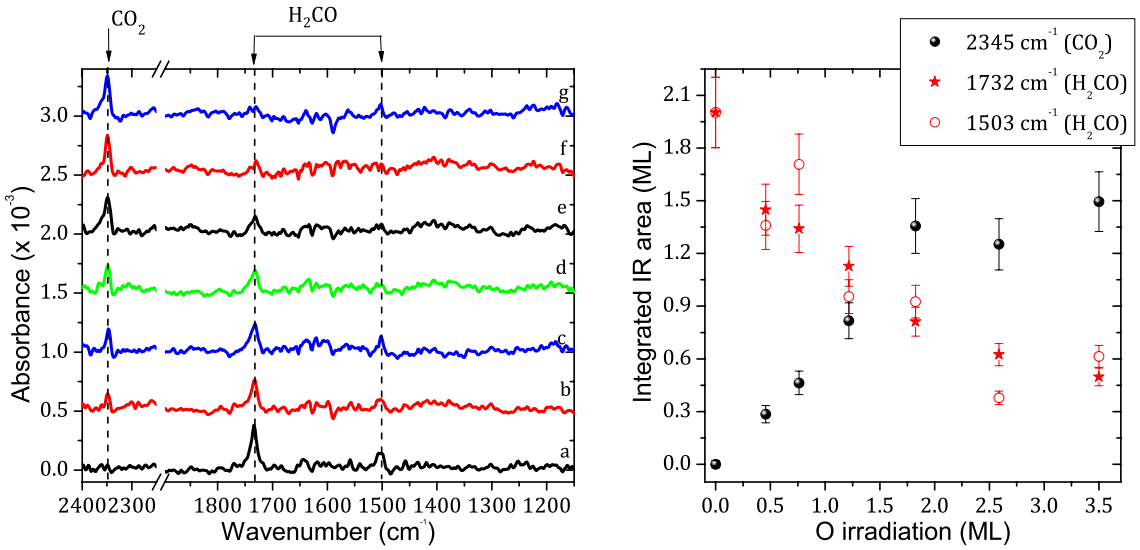

Fig. 6. *Left panel*: seven RAIR spectra obtained after deposition of (a) 2 ± 0.5 ML of H_2CO; (b) 2 ± 0.5 ML of H_2CO + 0.5 ± 0.1 ML of O atoms; (c) 2 ± 0.5 ML of H_2CO + 0.8 ± 0.1 ML of O atoms; (d) 2 ± 0.5 ML of H_2CO + 1.2 ± 0.2 ML of O atoms; (e) 2 ± 0.5 ML of H_2CO + 2.0 ± 0.3 ML of O atoms; (f) 2 ± 0.5 ML of H_2CO + 2.8 ± 0.3 ML of O atoms; (g) 2 ± 0.5 ML of H_2CO + 3.8 ± 0.3 ML of O atoms, on a ASW ice held at 55 K (H_2CO was always deposited at 60 K). *Right Panel*: integrated areas of the H_2CO and CO_2 bands as a function of O-atom dose.

with H_2CO and form CO_2([O_3] ≈ [CO_2]), owing to the lack of O_2 and the lower mobility of O atoms.

3.2. Temperature effects: O-atom irradiation at 55 K

Minissale et al. (2013b, 2014) show that solid-state formation of O_3 is efficient at temperatures lower than 55 K. In fact, temperatures higher than 55 K prevent O_2 adsorption on the surface so O_3 can no longer be formed. Figures 4 and 5 show that O_3 is the main product after H_2CO is exposed to O atoms. To avoid O_3 formation, we thus sent O atoms onto H_2CO ice held at 55 K. Figure 6 shows seven RAIR spectra after O irradiation of 2 ± 0.5 ML of H_2CO, previously adsorbed on ASW, at 55 K (from curve a to g, 0, 0.5, 0.8, 1.2, 2, 3.8 ML of O, respectively, were sent onto H_2CO). The right-hand panel of Fig. 6 shows the integrated areas of the bands at 1732 and 1502 cm^{-1} of H_2CO (triangles and circles, respectively) and the one at 2345 cm^{-1} of CO_2 (black circles). The spectra of Fig. 6 differ from those in Fig. 5 for two main features: the O_3 band is not present and the band at 2347 cm^{-1} (CO_2) increases steadily with O-exposure time. These two main differences, as discussed in detail in the model section, facilitate the evaluation of the H_2CO + O activation barrier.

3.3. Experiments with isotopologues

To confirm the results presented above and for a better understanding of the solid state reaction network, we also performed experiments using another isotopologue of formadehyde, D_2CO. Further experiments in which $H_2^{13}CO$ was used are described in Appendix A.

The top panel of Fig. 7 shows three RAIR spectra recorded after deposition of oxygen atoms (0, 1.4, and 3.8 ML from curves a to c, respectively) on 2 ± 0.5 ML of D_2CO held at 55 K. Three spectral features are apparent. D_2CO is detected through the CO stretch mode at 1680 cm^{-1} (decreasing in intensity from a to c) and the asymmetric stretch of CD_2 at 2154 cm^{-1}; the latter is visible only in spectrum a; the third feature at 2359 cm^{-1} is due to the antisymmetric stretch of CO_2 and increases in intensity

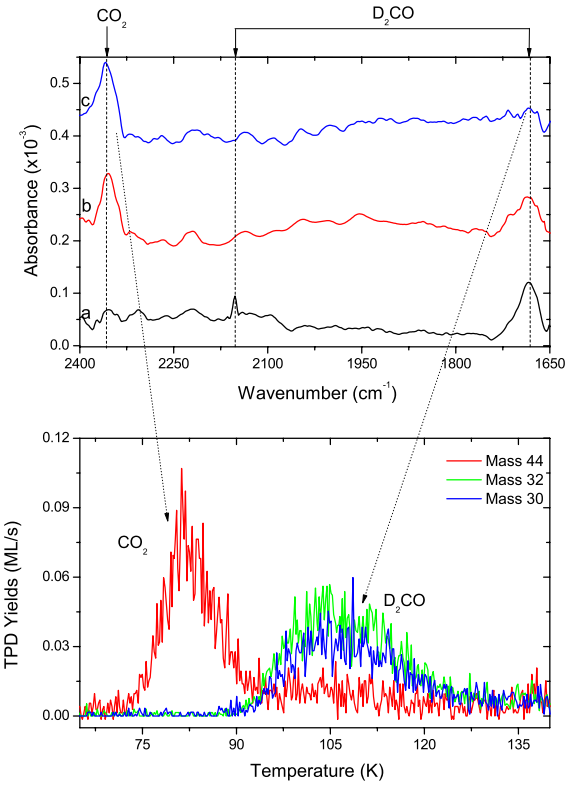

Fig. 7. *Top panel*: three RAIR spectra obtained after deposition of (a) 2±0.5 ML of D_2CO; (b) 2±0.5 ML of D_2CO+1.4±0.1 ML of O atoms; (c) 2 ± 0.5 ML of D_2CO + 3.8 ± 0.3 ML of O atoms, on oxidised HOPG held at 60 K. *Bottom panel*: CO_2 (via mass 44) and D_2CO (via masses 32 and 30) TPD mass spectra obtained after deposition of 2 ± 0.5 ML of D_2CO + 3.8 ± 0.3 ML of O atoms on oxidised HOPG held at 60 K.

from spectrum a to spectrum c. Also, a very weak band due to O_3 is visible at 1043 cm^{-1} (not shown). The TPD traces in the bottom panel were obtained after deposition of 2 ± 0.5 ML of D_2CO + 3.8 ± 0.3 ML of O atoms on ASW ice. Newly formed CO_2 desorbs between 70 and 90 K and is detected via mass 44.

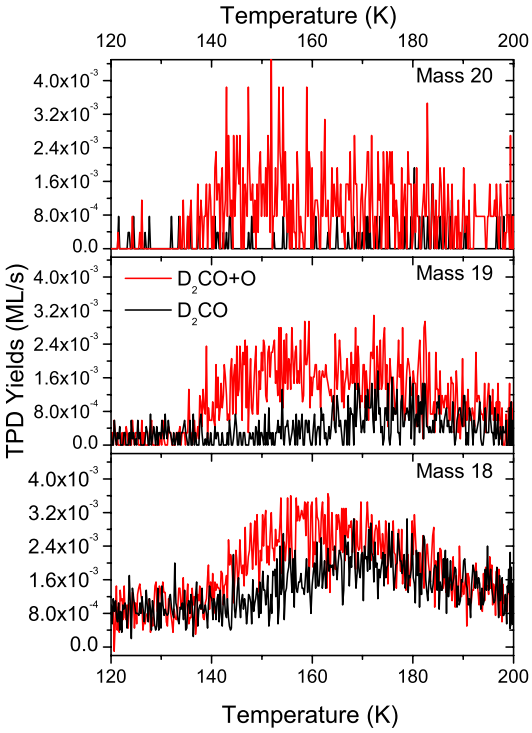

Fig. 8. TPD traces of mass 18, 19, and 20 obtained after deposition of 2 ± 0.5 ML of D_2CO (black curves) and 2 ± 0.5 ML of D_2CO + 3.8 ± 0.3 ML of O atoms (red curves) on oxidised HOPG held at 60 K.

The fraction of D_2CO molecules that did not react desorb between 85 K and 140 K and are detected via the fragments D_2CO^+ (mass 32) and DCO^+ (mass 30). TPD results corroborate the previous spectral assignments of the infrared bands and give additional information. Figure 8 shows TPD traces of mass 18, 19, and 20 between 130 and 200 K. The black lines represent TPDs after deposition of 2 ± 0.5 ML of D_2CO on oxidised HOPG held at 55 K, while red lines were obtained by irradiating the same amount of D_2CO with 3.8 ± 0.3 ML of O. The signal at mass 20 comes from the ionisation of heavy water (D_2O^+): it is almost zero in the black curve, while it has a peak in the red curve. Mass 19 (HDO^+ and 18 (H_2O^+ and OD^+) signals are present in both cases, even if the peak areas of the red curve are twice bigger than the peaks of the black curve. These mass spectra support the formation of D_2O after D_2CO oxygenation. We discuss this point extensively in the next section.

4. Model and discussion

4.1. Quantum chemical calculations on the O + H_2CO reaction

The focus of this paper is on the investigation of solid-state reactions involving formaldehyde ices and oxygen atoms at low temperatures. All the experiments presented in Sect. 3 show that when formaldehyde is exposed to O atoms, H_2CO is consumed and CO_2 is formed. In this section, we describe quantum chemical calculations on O + H_2CO reaction in detail. However, we have used prevalently gas-phase energetic data to carry out our calculations. We would like to stress that solid-state reactivity is somewhat different than the gas-phase one, because of interactions between adsorbate and adsorbent. For this reason, the goal of our quantum chemical calculations is essentially to provide a first estimation of the trend of the different channels studied. The energetic data, present in this section, have to be taken just as qualitative values, since they would be substantially influenced by the solid-state phase chemistry.

Our experimental results are very similar to those obtained by different experimental groups at high (>300 K) temperature in gas phase, i.e. Chang & Barker (1979) and Wellman et al. (1991). Chang & Barker (1979) proposed that CO_2 formation occurs in the following steps:

1. O-atom addition to the doubly-bonded carbon atom in H_2CO and the following formation of a vibrationally excited triplet of methylenebis(oxy) (H_2CO_2);
2. H_2CO_2 is formed in the $^3B_2$ state, and owing to a hydrogen shift, it forms vibrationally excited formic acid (H-atom migration process);
3. Once formed, the triplet formic acid is decomposed by several pathways (HCO+OH, HCO_2+H, HOCO+H);
4. Further fragmentation of HOCO and HCO_2 or oxygenation of HCO would lead to CO_2 formation.

On the other hand, Wellman et al. (1991) proposed that H_2CO+O proceeds via a direct hydrogen abstraction (H_2CO+O→OH+HCO), and a secondary reaction of oxygen atoms with HCO may lead to CO_2 formation. In the gas phase, despite some ambiguities, the reaction mainly leads to abstraction products, HCO + OH, through a barrier measured as equal to 1540 K (Klemm 1979; Klemm et al. 1980), with a CO_2 product-branching ratio inferior to 5% (Wellman et al. 1991). We stress that neither Chang & Barker (1979) nor Wellman et al. (1991) have shown direct measurements of HCOOH and HCO. This is consistent with our experimental results. Theoretical calculations (Dupuis & Lester 1984) show that CO_2 production via the addition channel ($^3OCH_2O$, second reaction) should be unlikely, since it involves a transition state above the O + H_2CO entrance channel. Moreover, H_2CO+O could lead to the formation of the Criegee species (CH_2OO) in its triplet state. Nevertheless, we can neglect this channel in our system, thanks to its wide endothermicity (+115 kJ/mol, see Table C.2).

To understand how CO_2 is formed in our system, we carried out a series of DFT calculations (see Appendix C for details). We suppose that H_2CO+O can lead to various products:

$$^1H_2CO + {}^3O \rightarrow {}^2OH + {}^2HCO \qquad \Delta H = -60 \text{ kJ/mol} \quad (3)$$

$$\rightarrow {}^3OCH_2O \qquad \Delta H = -80/-70 \text{ kJ/mol} \quad (4)$$

where enthalpies of reactions have been taken from the literature (Baulch et al. 2005, for the first reaction; Dupuis & Lester 1984, for the second value of second reaction) or evaluated in the present work.

In the case of surface reaction (i.e., ice or graphite), the surface interactions have a complex effect on barrier heights (Bromley et al. 2014). For the H + H_2CO reaction on water ice, a small reduction (≈130 K) in the activation barrier was calculated for the addition reaction, while the barrier for abstraction reaction was increased significantly (increased by 725 K) (Goumans 2011). It is reasonable to imagine that the O reaction with H_2CO ice presents a similar effect. To get a better picture of the various mechanisms, we performed theoretical calculations using the *Gaussian 09*[3] package. Calculations details are presented in Appendix C. The energy diagram calculated for the first step of the O + H_2CO reaction (energy values are close to the CCSD(T)/cc-pVTZ and MP2/cc-pVTZ values including zero-point energies, ZPE) is presented in Fig. 9. The reaction

[3] http://www.gaussian.com/g_prod/g09.htm

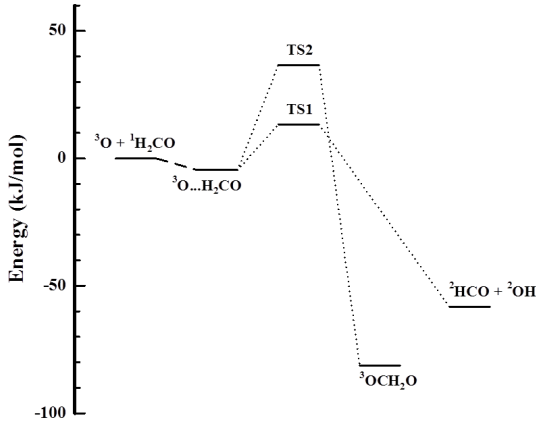

Fig. 9. Relative energy diagram for the O + H_2CO reaction.

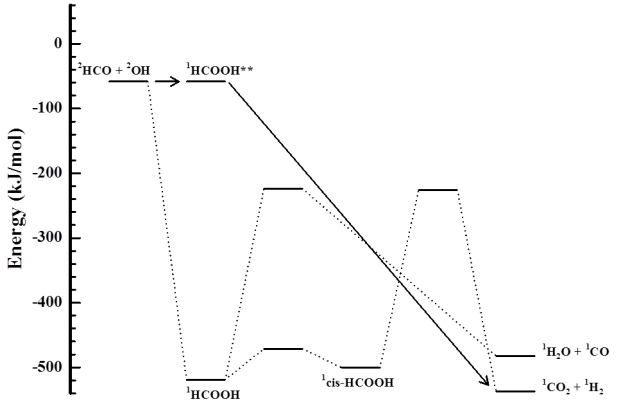

Fig. 10. Relative energy diagram for the HCOOH decomposition calculated at M06-2X/cc-pVTZ level.

pathway is initiated by the formation of a pre-reactive complex (PRC) O . . . H_2CO corresponding to a long-range interaction between O atom and H_2CO.

From the PRC, two reactive pathways have been found, one leading to OH + HCO formation through a transition state for H atom abstraction, TS1, and the other leading to oxygen atom addition through TS2 transition state. The energy barrier for the H-atom abstraction depends on the calculation level, ranging from 1 kJ/mol at M06-2X level to 39 kJ/mol at MP2 level and equal to 21 kJ/mol at CCSD(T) level, and the energy barrier for the oxygen atom addition ranging from 30 kJ/mol at M06-2X level to 93 kJ/mol at MP2 level and equal to 53 kJ/mol at CCSD(T) level. Calculations show that in the gas phase, the reaction happens mainly through H atom abstraction with a barrier around 10−20 kJ/mol. They are qualitatively in good agreement with observations, considering that DFT with M06-2X method underestimates the barrier height and MP2 overestimates the barrier (Loison et al. 2014, 2014b). In the case of oxygen-atom addition, it is very unlikely that surface interactions have such an effect on the addition barrier to make this channel important. Moreover, tunneling should be efficient for H-atom abstraction and less efficient for O-atom addition.

The main exit channel for O atom reaction with H_2CO on a cold surface is very likely HCO + OH. The newly formed HCO and OH should have low kinetic energy owing to

- low exothermicity of reaction;
- large amount of available energy localized into vibrational and rotational degrees of freedom.

Probably, HCO and OH will then stay relatively close on the surface and should mainly recombine on the singlet surface (^{2}HCO +^{2} OH correlate with singlet and triplet surface) without barrier, leading to excited HCOOH**. If some OH and HCO can move on the surface, OH will quickly react with H_2CO leading to H_2O + HCO (Xu et al. 2006; Yetter et al. 1989). The low amount of water formed in the experiments is a strong indication that OH does not move on the surface but rather form HCOOH**. We performed theoretical calculations at the M06-2X level to characterise stationary points in the HCOOH* evolution. Our results (in good agreement with previous calculations for the HCOOH dissociation, Chang et al. 2007) are presented in Fig. 10. Theoretical calculations on energy transfer from HCOOH* toward phonon modes of the ice is far beyond the scope of this article (and is also far from being well understood). HCOOH* has an internal energy equal to 460 kJ/mol corresponding to the strength of the OC(H)-OH bond, so well above the dissociation barrier towards H_2 + CO_2 and H_2O + CO.

To estimate the evolution of excited HCOOH** and its unimolecular decomposition, we use our experimental results showing that neither HCOOH nor H_2O were formed and then we mainly consider CO_2 + H_2 formation. That CO_2 + H_2 is favoured is in good agreement with theoretical calculations for the H+HOCO reaction (Yu & Francisco 2008) leading to similar HCOOH** energized adducts. The most surprising experimental result is the low amount of HCOOH stabilized, which should be a function of energy relaxation efficiency through surface interaction. The low efficiency of HCOOH stabilization in our experiments clearly shows the complexity of surface reactions, and it is definitively an important experimental result because the competition between adduct stabilization and bimolecular exit channel happens for a majority of surface reactions (i.e., C + NO → CN+O/CO+N/CNO/NCO, CH+CH_4 → C_2H_5/C_2H_5+H, H+HO_2 → H_2O_2/OH + OH/H_2 + O_2, H_2O + O, and so on). We propose the following simplified chemical pathways:

a.1) $H_2CO + O \rightarrow (OH + HCO)_{cage}$
a.2) $(OH + HCO)_{cage} \rightarrow HCOOH^{**}$
a.3) $HCOOH^{**} \rightarrow (CO_2 + H_2)$ or $(H_2O + CO)$
b) $O + O \rightarrow O_2$
c) $O_2 + O \rightarrow O_3$
d) $O + CO \rightarrow CO_2$

where reaction a1 has a barrier of 335 K (fitted using E_{Odiff} = 700 K, see previous section). Reactions a2 (radical-radical reaction), b, and c have no barrier; reaction a3 presents a 95%−5% (±5%) branching ratio; and reaction d presents a barrier of 600 K (Minissale et al. 2013a).

In the next section, we describe the model used to evaluate the activation barrier of the H_2CO + O reaction.

4.2. Evaluation of the H_2CO+O barrier

In this section we present the model used to fit our experimental data and, in particular, to evaluate the activation barrier of the H_2CO + O reaction. The model is composed of a set of five differential equations that account for the surface population of H_2CO, O atoms, O_2, O_2, and CO_2 (see Appendix B for further details). In fact, we considered only the most abundant species present on the surface, and the three main reaction pathways:

a) $H_2CO + O \rightarrow CO_2 + H_2$
b) $O + O \rightarrow O_2$
c) $O_2 + O \rightarrow O_3$.

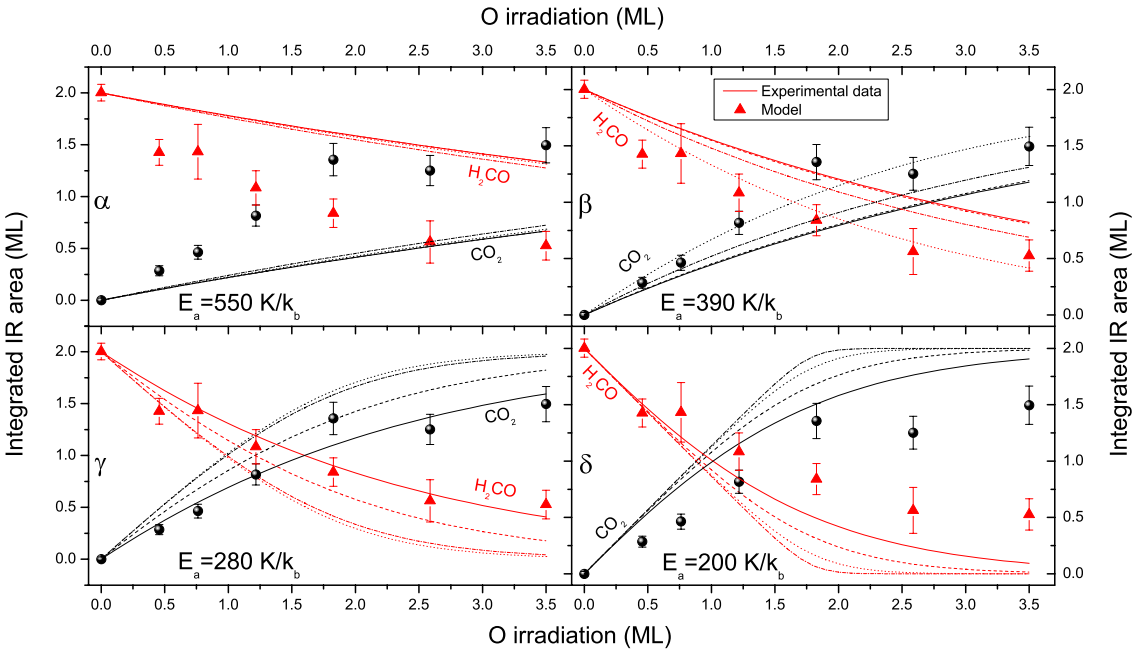

Fig. 11. Comparison between model (lines) and experimental data (symbols); IR yields of H_2CO (red) and CO_2 (black) are shown as a function of O-atom coverage. Four values of E_{Odiff} are used: 900 K/k_b (solid line), 800 K/k_b (dashed line), 700 K/k_b (dotted line), 600 K/k_b (dashed-dotted line). From panels α to δ, E_a is 550 K/k_b, 390 K/k_b, 280 K/k_b, and 200 K/k_b, respectively.

H_2 was not included in our model, since our experiments were performed at high surface temperature and H_2 has a very short residence time under these conditions. In any case, H_2 is inert at low temperature and cannot affect the surface density of other species. The surface reactions listed above can occur through two mechanisms: the Eley-Rideal (ER) and the Langmuir-Hinshelwood (LH) mechanisms. In the ER mechanism one molecule is already adsorbed on the surface, and the other comes from the gas phase (i.e., the beam line). The ER becomes more efficient as the surface coverage increases. In the LH mechanism, both molecules are physisorbed to the surface, and they can meet each other by diffusing on the surface and eventually react. LH is highly dependent on the surface temperature. With these considerations in mind, we chose to fit the data of Fig. 6 (right panel) to give a more precise evaluation of the H_2CO+O activation barrier. Actually, the physicochemical conditions in these experiments allow us to simplify our model and reduce the errors:

- O-atom diffusion is very fast, and the majority of adsorbed O atoms are consumed through reaction (b);
- reaction (c) can be neglected, since it is impeded by O_2 desorption[4];
- reaction (a) is more likely to occur via ER, since O atoms are deposited on the H_2CO ice.

Clearly the last point does not exclude that reaction (a) could occur via the LH mechanism, and this actually represents the main source of error in the barrier determination. The LH mechanism depends strongly on the O-atom diffusion barrier (E_{Odiff}), one of the free parameters of the model. The barrier E_{Odiff} is a pure thermal diffusion barrier since quantum effects are negligible at high temperatures (Minissale et al. 2013a), and it has an upper limit of 900 K/k_b (Cazaux et al. 2010) and a lower limit given by ozone formation in our experiments (<0.05 ML). A value lower than 600 K/k_b for E_{Odiff} increases the efficiency of reaction (b) and produces more than 0.05 ML of ozone. Within these two boundaries, the total amount of CO_2 formed via LH changes by 20%, if E_{Odiff} = 900 K/k_b, or 5%, if E_{Odiff} = 600 K/k_b. This indetermination, as we see below, complicates the evaluation of the activation barrier E_a of reaction (a), the second free parameter of the model. A priori, E_a is a positive real number and becomes zero in the case of a barrierless reaction. Figure 11 shows the results of the model (lines) compared with experimental data. We used four values for E_a: 550 K/k_b (panel α), 390 K/k_b (panel β), 280 K/k_b (panel γ), and 200 K/k_b (panel δ). We varied E_{Odiff} in the 600–900 K/k_b range, and Fig. 11 shows the four cases: 600, 700, 800, and 900 K/k_b. Panel α shows that a value of E_a that is too high (>550 K/k_b) is not able to fit our data for any value of E_{Odiff}: small amounts of CO_2 are formed, small amounts H_2CO are consumed, and a large amount of ozone is formed. On the other hand, a value that is too small (<200 K/k_b) for E_a has an opposite effect, CO_2 is formed too rapidly and H_2CO is consumed too quickly by O atoms (panel δ). Couples of values of E_a and E_{Odiff} ranging in 390–280 K/k_b and 600–900 K/k_b, respectively (panels β and γ), give an excellent fit to the experimental data. Because the fit depends on two parameters, we are not able to give a precise value of the activation barrier of reaction (a). However, we have to stress that a given choice of E_{Odiff}, automatically determines the value of E_a: by using E_{Odiff} = 700 ± 150 K/k_b, we found E_a = 335 ± 55 K/k_b.

The activation barrier that we have found for solid state reaction H_2CO+O (>300 K) is lower than gas phase barrier (>1560 K, Wellman et al. 1991). The reason for such a low activation barrier is probably the catalytic effect of the surface.

5. Astrophysical conclusions

In this paper we have shown that O(^{3}P) atoms are able to react with H_2CO on cold surfaces, such as amorphous water or oxidised graphite, under conditions encountered in interstellar

[4] From preliminary experiments, we determined that atomic oxygen has a long residence time (with respect to the experimental timescales) even at 55 K.

dense clouds. Using a model, we estimated a value of 335 ± 55 K/k_b for its activation barrier, and CO_2 was found to be the main product of the reaction. This reaction is relevant to astrochemistry because it may account for CO_2 abundances, as well as for CH_3OH ones, in interstellar ices. Actually, carbon dioxide is one of the most common and abundant types of ice, and it has been detected in many interstellar environments, from comets (Ootsubo et al. 2010) to other galaxies (Shimonishi et al. 2010; Oliveira et al. 2011). Its high abundances observed in interstellar ices are explained through some solid-phase reactions. Energetic formation processes leading to efficient formation of CO_2 include irradiation of CO ices (pure or mixed with H_2O) with photons, charged particles or electrons (Ioppolo et al. 2009; Laffon et al. 2010). On the other hand, Whittet et al. (1998) invoke chemical pathways occurring without the addition of energy to explain the CO_2 detection in those interstellar environments where a lack of UV photons forbids ice processing (i.e., molecular cloud Taurus). To date, only two (non energetic) pathways were considered:

d) $CO + O \rightarrow CO_2$
e) $CO + OH \rightarrow CO_2 + H$.

Roser et al. (2001) and Raut & Baragiola (2011) successfully showed that the formation of CO_2 is possible through reaction (d). Recently, Minissale et al. (2013b) have confirmed these results and estimated an activation barrier of about 600 K/k_b. Recently, Noble et al. (2011) and Oba et al. (2011) have shown experimentally the CO_2 formation through reaction (e), but no consistent values were obtained for the activation barrier. In this paper, we showed that also reaction (a) (H_2CO+O → CO_2+H_2) can efficiently form CO_2 in the ISM. Moreover, this reaction can help to explain the CH_3OH abundances variability (from <3% to 25−30% with respect to water) in interstellar ices (Dartois et al. 1999; Whittet et al. 2011). Formation of CO_2 and CH_3OH in "hot" environments (high UV fluxes or/and T_{grain} > 50 K) can be explained through energetic processing of icy mantles (Moore & Hudson 1999; Ioppolo et al. 2009, and references therein), but as opposed to CO_2, CH_3OH formation is strongly dependent on the ice composition.

In cold environments, where energetic routes are not efficient, methanol and carbon dioxide are believed to form via the solid state reactions shown in Fig. 12 and listed in Table 4. In summary, we can say that:

- CH_3OH is formed via four CO hydrogenations (with a total energy barrier >800 K/k_b, Fuchs et al. 2009), leading to the formation of two unstable products, HCO and CH_3O, and one stable molecule, namely H_2CO;
- CO_2 is formed following three different chemical pathways: reaction (a), (d), and (e);
- H_2CO is a precursor not only of CH_3OH, but also of CO_2.

These considerations can have two consequences for the CH_3OH/CO_2 ratio in interstellar ice: (1) where large abundances of atomic oxygen (O/H ratio >0.1) are observed (i.e., Sgr B2 and L1689N2), the CH_3OH/CO_2 ratio tends to zero; (2) where low O/H ratios (<0.1) are observed, the increase in CH_3OH/CO_2 ratio is difficult to predict a priori because it may depend on other factors. For example, the large CO hydrogenation energy barrier and H_2CO+O reaction could hinder CH_3OH formation and favour CO_2 formation.

Acknowledgements. The LERMA-LAMAp team in Cergy acknowledges the support of the national PCMI programme founded by CNRS. M.M. acknowledges financial support by LASSIE, a European FP7 ITN Community's Seventh Framework Programme under Grant Agreement No. 238258. M.M. also thanks Dr. M. E. Palumbo and Dr. E. Dartois for fruitful discussions.

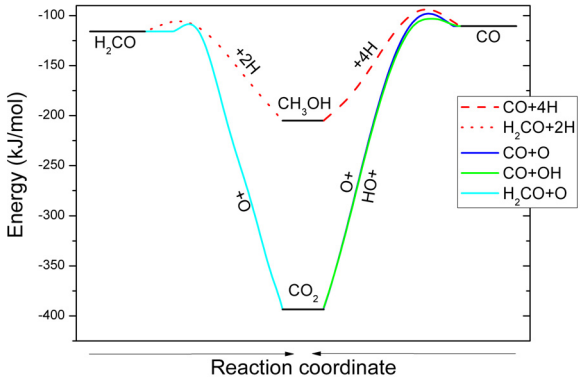

Fig. 12. Energetics of the CO+H/O reaction pathways. The enthalpies of CO_2 and CH_3OH and the activation barrier of each reaction are listed in Table 3. The enthalpies of H_2CO and CO are −115.9 and −110.5 kJ/mol, respecively (http://webbook.nist.gov/chemistry/).

Table 4. List of solid state reactions and their activation barriers to form CO_2 and CH_3OH.

Molecule	Enthalpy (kJ/mol)	Reaction	Activation barrier (kJ/mol)	(K/k_b)
CO_2	−393[a]	CO+O	5.1[b]	630[b]
		CO+OH	≤3.3[c]	0−400[c]
		H_2CO+O	2.8[d]	335[d]
CH_3OH	−205[a]	CO+4H	≥6.6[e]	≥800[e]
		H_2CO+2H	≥3.3[e]	≥400[e]

Notes. [(a)] NIST Chemistry WebBook (http://webbook.nist.gov/chemistry/); [(b)] Minissale et al. (2013b) ; [(c)] Oba et al. (2011), Noble et al. (2011) ; [(d)] This work ; [(e)] Fuchs et al. (2009).

References

Allamandola, L. J., Sandford, S. A., & Valero, G. J. 1988, Icarus, 76, 225
Amiaud, L., Fillion, J.-H., Baouche, S., et al. 2006, J. Chem. Phys., 124, 094702
Amiaud, L., Dulieu, F., Fillion, J.-H., Momeni, A., & Lemaire, J. L. 2007, J. Chem. Phys., 127, 144709
Baulch, D. L., Bowman, C. T., Cobos, C. J., et al. 2005, J. Phys. Chem. Ref. Data, 34, 757
Boogert, A. C. A., Pontoppidan, K. M., Knez, C., et al. 2008, ApJ, 678, 985
Braslavsky, S., & Heicklen, J., 1976, Int. J. Chem. Kinet., 8, 801
Bromley, S. T., Goumans, F., Herbst, E., Jones, A., & Slater, B. 2014, Phys. Chem. Chem. Phys., 16, 18623
Cazaux, S., Cobut, V., Marseille, M., Spaans, M., & Caselli, P. 2010, A&A, 74, A522
Chang, J. S., & Barker, J. R., 1979, JPC, 83, 3059
Chang, J.-G., Chen, H.-T., Xu, S., & Lin, M. C. 2007, J. Phys. Chem. A, 111, 6789
Congiu, E., Matar, E., Kristensen, L. E., Dulieu, F., Lemaire, J. L. 2009, MNRAS, 397, L96
Congiu, E., Chaabouni, H., Laon, C., et al. 2012, J. Chem. Phys., 137, 054713
Congiu, E., Minissale, M., Baouche, S., et al. 2014, Faraday Discussion, 168, 151
Crovisier, J., & Bockeleé-Morvan, D. 1999, Space Sci. Rev., 90, 19
Dartois, E. 2005, Space Sci. Rev., 119, 293
Dartois, E., Schutte, W., Geballe, T. R., et al. 1999, A&A, 342, L32
Davies, R. D., & Few, R. W., 1979, IAU Symp., 84, 81
Downes, D., Wilson, T. L., Bieging, J., & Wink, J. 1980, A&AS, 40, 379
Dulieu, F., Congiu, E., Noble, J. 2013, Scientific Rep., 3, 1338
Dunning, Jr., T. H. 1989, J. Chem. Phys., 90, 1007
Dupuis, M., & Lester, W. A. 1984, J. Chem. Phys., 80, 4193
Fuchs, G. W., Cuppen, H. M., Ioppolo, S., et al. 2009, A&A, 505, 629
Goumans, T. P. M. 2011, MNRAS, 413, 2615
Hiraoka, K., Ohashi, N., Kihara, Y., et al. 1994, Chem. Phys. Lett., 229, 408
Hidaka, H., Watanabe, N., Shiraki, T., Nagaoka, A., & Kouchi, A. 2004, ApJ, 614, 1124

Hudson, R. L., & Moore, H. M. 1999, Icarus, 140, 451
Ioppolo, S., Palumbo, M. E., Baratta, G. A., & Mennella, V. 2009, A&A, 493, 1017
Keane, J. V., Tielens, A. G. G. M., Boogert, A. C. A., Schutte, W. A., & Whittet, D. C. B. 2001, A&A, 376, 254
Klemm, R. B. 1979, J. Chem. Phys., 71, 1987
Klemm, R. B., Skolnik, E. G., & Michael, J. V. 1980, J. Chem. Phys., 72, 1256
Laffon, C., Lasne, J., Bournel, F., et al. 2010, Phys. Chem. Chem. Phys., 12, 10865
Loison, J.-C., Wakelam, V., Hickson, K. M., Bergeat, A., & Mereau, R. 2014a, MNRAS, 437, 930
Loison, J. C., Hickson, K. M., & Wakelam, V. 2014b, MNRAS, 443, 398
Maret, S., Ceccarelli, C., Caux, E., et al. 2004, A&A, 416, 577
Madzunkov, S. M., MacAskill, J. A., Chutjian, A., et al. 2009, ApJ, 697, 801
Michael, J. V., Kumaran, S. S., & Su, M.-C. J. 1999, Phys. Chem. A, 103, 5942
Minissale, M. 2014, Ph.D. Thesis, University of Cergy-Pontoise, France, available at http://www.u-cergy.fr/_attachments/theses-soutenues-au-lamap-article/Marco_MINISSALE_2014.pdf?download=true
Minissale, M., & Dulieu, F. 2014, J. Chem. Phys., 141, 014304
Minissale, M., Congiu, E., Baouche, S., et al. 2013a, Phys. Rev. Lett., 111, 053201
Minissale, M., Congiu, E., Manicò, G., Pirronello, V., & Dulieu, F. 2013b, A&A, 559, A49
Minissale, M., Congiu, E., & Dulieu, F. 2014, J. Chem. Phys., 140, 074705
Mispelaer, F., Theulé, P., Aouididi, H., et al. 2013, A&A, 555, A13
Mumma, M. J., DiSanti, M. A., Magee-Sauer, K., et al. 2005, Science, 310, 270
Noble J. A., Dulieu F., Congiu E., & Fraser H. J. 2011, ApJ, 735, 121
Noble J. A., Congiu E., Dulieu F., & Fraser H. J. 2012a, MNRAS, 421, 768
Noble, J., Theule, P., Mispelaer, F., et al. 2012b, A&A, 543, A5
Oba, Y., Watanabe, N. Kouchi, A., Hama, T., & Pirronello, V. 2011, Phys. Chem. Chem. Phys., 13, 15792
Oliveira, J. M., van Loon, J. Th., Sloan, G. C., et al. 2011, MNRAS, 411, L36
Ootsubo, T., Usui, F., Kawakita, H., et al. 2010, ApJ, 717, L66
Raut, U., & Baragiola, R., ApJ, 737, L14
Rimola, A., Taquet, V., Ugliengo, P., Balucani, N., & Ceccarelli, C. 2014, A&A, 572, A70
Roser, J. E., Vidali, G., Manicó, G., & Pirronello, V. 2001, ApJ, 555, L61
Shalabiea, O. M., & Greenberg, J. M. 1994, A&A, 290, 266
Shimonishi, T., Onaka, T., Kato, D., et al. 2010, A&A, 514, A12
Schutte, W. A., Allamandola, L. J., & Sandford, S. A. 1993a, Science, 259, 1143
Schutte, W. A., Allamandola, L. J., & Sandford, S. A. 1993b, Icarus, 104, 118
Schutte, W. A., Gerakines, P. A., Geballe, T. R., et al. 1996, A&A, 309, 633
Snyder, L. E., Buhl, D., Zuckerman, B., & Palmer, P. 1969, Phys. Rev. Lett., 22, 679
Tang, X. D., Esimbek, J., Zhou, J. J., et al. 2013, A&A, 551, A28
Theulé, P., Duvernay, F., Danger, G., et al. 2013, Adv. Space Res., 52, 1567
Watanabe, N., & Kouchi, A. 2002, ApJ, 571, L173
Watanabe, N, Mouri, O., Nagaoka, A., et al. 2007, ApJ, 668, 1001
Wellman, J., Park, J., & Hershberger, J. F. 1991, Chem. Phys. Lett., 178, 405
Whittet, D. C. B., Geralines, P. A., Tielens, A. G. G. A., et al. 1998, ApJ, 498, L159
Whittet, D. C. B., Cook, A. M., Herbst, E, Chiar, J. E., & Shenoy, S. S. 2011, ApJ, 742, 28
Xu, S., Zhu, R. S., & Lin, M. C. 2006, Int. J. Chem. Kinet., 38, 322
Yetter, R. A., Rabitz, H., Dryer, F. L., Maki, R., G., & Klemm, R. B. 1989, J. Chem. Phys., 91, 4088
Yu, H.-G., & Francisco, J. S. 2008, J. Chem. Phys., 128, 4315
Zhao, Y., & Truhlar, D. 2008, Theor. Chem. Accounts, 120, 215
Zuckerman, B., Buhl, D., Palmer, P., & Snyder, L. E. 1970, ApJ, 160, 485

Pages 11 to 12 are available in the electronic edition of the journal at http://www.aanda.org

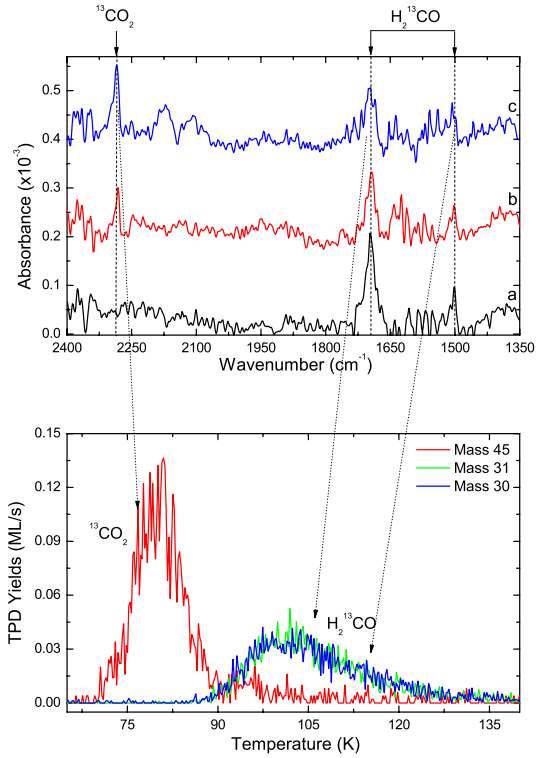

Fig. A.1. *Top panel*: three RAIR spectra obtained after deposition of (a) 2 ± 0.5 ML of $H_2^{13}CO$; (b) 2 ± 0.5 ML of $H_2^{13}CO$ + 1.4 ± 0.1 ML of O atoms; (c) 2 ± 0.5 ML of $H_2^{13}CO$ + 3.8 ± 0.3 ML of O atoms on oxidised HOPG held at 60 K. *Bottom panel*: $^{13}CO_2$ (via mass 45) and $H_2^{13}CO$ (via masses 31 and 30) TPD traces obtained after deposition of 2 ± 0.5 ML of $H_2^{13}CO$ + 3.8 ± 0.3 ML of O atoms on oxidised HOPG.

Appendix A: Additional experiments

To validate the formation of carbon dioxide, we performed further experiments using the $H_2^{13}CO$ isotopologue of formaldehyde: the results are presented below. The top panel in Fig. A.1 shows three RAIR spectra recorded after irradiation of 2 ± 0.5 ML of $H_2^{13}CO$ with increasing doses of oxygen atoms (0, 1.4, and 3.8 ML, respectively from a to c spectra) on oxidised HOPG at 55 K. Three main features are visible: at 1502 and 1697 cm^{-1} due to $H_2^{13}CO$, $^{13}CH_2$ scissoring and ^{13}CO stretch mode, respectively; at 2285 cm^{-1} due to the antisymmetric stretch of $^{13}CO_2$. Moreover, a very weak band due to O_3 is present at 1042 cm^{-1} (not shown). Each IR band varies in intensity from curve to curve. In particular, the $H_2^{13}CO$ bands decrease from spectrum a to spectrum c, and the reverse occurs to the bands of $^{13}CO_2$. This indicates that $H_2^{13}CO$ is consumed and $^{13}CO_2$ is formed subsequently to O irradiation. The infrared assignments are confirmed by TPD results shown in the bottom panel of Fig. A.1. These TPD traces were obtained after deposition of 2 ± 0.5 ML of $H_2^{13}CO$ + 3.8 ± 0.3 ML of O atoms on oxidised HOPG held at 60 K. Newly formed $^{13}CO_2$ desorbs between 70 and 90 K and is detected via mass 45. Unreacted $H_2^{13}CO$ molecules desorb between 85 and 140 K and are detected via two fragments: $^+H_2^{13}CO$ (mass 31) and $^+H^{13}CO$ (mass 30).

Appendix B: Rate equations

The model used to fit our experimental data is very similar to the one described in Minissale (2014) and Minissale et al. (2013b, 2014). It is composed of five differential equations, one for each of the species considered: H_2CO molecules, deposited on the surface; O atoms, coming exclusively from the beam; O_3 and CO_2, formed only on the surface; and finally O_2, coming both from the beam and formed on the surface. Each differential equation is composed of different terms:

- positive terms indicate a contribution to the increase in the surface density of the species, i.e., a molecule (or atom) arrives from the gas phase or is formed on the surface;
- negative terms indicate a decrease in the surface density of the species, i.e., a molecule (or atom) is consumed on the surface or desorbs and returns to the gas phase.

Likewise, the terms involving the ER and LH mechanisms are independent of one another, thus we are able to determine the amount of a species formed (or consumed) via the ER or the LH mechanism. For the sake of simplicity, the differential equations were divided into two sets, accounting for the two formation mechanism separately. Below is the list of equations governing the CO_2 formation by the ER mechanism:

$$\mathrm{O}'(t) = 2\tau\,\phi_{\mathrm{O_2off}}\,(1 - 2\mathrm{O} - \mathrm{O_2}) - (1-\tau)\,\phi_{\mathrm{O_2off}}\,\mathrm{O} - r_{\mathrm{aER}}\,2\tau\phi_{\mathrm{O_2off}}\mathrm{H_2CO} - \mathrm{O}\,r_{\mathrm{Deso_O}} \quad \text{(B.1)}$$

$$\mathrm{O_2}'(t) = (1-\tau)\,\phi_{\mathrm{O_2off}}\,(1 - \mathrm{O}\,(1-\epsilon)) - 2\tau\,\phi_{\mathrm{O_2off}}\,\mathrm{O_2} + 2\tau\,(1-\epsilon)\,\phi_{\mathrm{O_2off}}\,\mathrm{O} - \mathrm{O_2}\,r_{\mathrm{Deso_{O_2}}} \quad \text{(B.2)}$$

$$\mathrm{O_3}'(t) = (1-\tau)\,\phi_{\mathrm{O_2off}}\,\mathrm{O} + 2\tau\,\phi_{\mathrm{O_2off}}\,\mathrm{O_2} \quad \text{(B.3)}$$

$$\mathrm{H_2CO}'(t) = -r_{\mathrm{aER}}\,2\tau\,\phi_{\mathrm{O_2off}}\,\mathrm{H_2CO} \quad \text{(B.4)}$$

$$\mathrm{CO_2}'(t) = r_{\mathrm{aER}}\,2\tau\,\phi_{\mathrm{O_2off}}\,\mathrm{H_2CO}. \quad \text{(B.5)}$$

O, O_2, O_3, H_2CO, and CO_2 are the surface densities (expressed in fractions of ML) of the species, τ is the dissociated fraction of O_2 defined in Sect. 2, $\phi_{\mathrm{O_2off}}$ is the flux (0.003 cm^{-2} s^{-1}) of O_2, ϵ is the evaporation probability – due to chemical desorption – of O_2 formed on the surface (Dulieu et al. 2013), and

$$r_{\mathrm{aER}} = \mathrm{e}^{-\frac{Ea}{T_{\mathrm{eff}}}} \quad \text{(B.6)}$$

$$r_{\mathrm{Deso_O}} = \nu\,\mathrm{e}^{\frac{-E_{\mathrm{Odes}}}{T}} \quad \text{(B.7)}$$

$$r_{\mathrm{Deso_{O_2}}} = \nu\,\mathrm{e}^{\frac{-E_{\mathrm{O_2des}}}{T}}, \quad \text{(B.8)}$$

are the reaction probability of H_2CO+O via ER and the desorption probabilities of O and O_2, respectively; $\nu = 10^{12}$ is the trial frequency for attempting a new event. Finally, simple calculations show that $2\tau\phi_{\mathrm{O_2off}}$ and $(1-\tau)\phi_{\mathrm{O_2off}}$ are the O and O_2 flux, respectively, when the discharge is on. Similarly, as for CO_2 formation by the LH mechanism, we have

$$\mathrm{O}'(t) = -4\,k_{\mathrm{Odiff}}\,\mathrm{O}\,\mathrm{O} - k_{\mathrm{Odiff}}\,\mathrm{O}\,\mathrm{O_2} - r_{\mathrm{aLH}}\,k_{\mathrm{Odiff}}\,\mathrm{OH_2CO} - \mathrm{O}\,r_{\mathrm{Deso_O}} \quad \text{(B.9)}$$

$$\mathrm{O_2}'(t) = 2\,k_{\mathrm{Odiff}}\,\mathrm{O}\,\mathrm{O}\,\epsilon - k_{\mathrm{Odiff}}\,\mathrm{O}\,\mathrm{O_2} - \mathrm{O_2}\,r_{\mathrm{Deso_{O_2}}} \quad \text{(B.10)}$$

$$\mathrm{O_3}'(t) = k_{\mathrm{Odiff}}\,\mathrm{O}\,\mathrm{O_2} \quad \text{(B.11)}$$

$$\mathrm{H_2CO}'(t) = -r_{\mathrm{aLH}}\,k_{\mathrm{Odiff}}\,\mathrm{O}\,\mathrm{H_2CO} \quad \text{(B.12)}$$

$$\mathrm{CO_2}'(t) = r_{\mathrm{aLH}}\,k_{\mathrm{Odiff}}\,\mathrm{O}\,\mathrm{H_2CO}, \quad \text{(B.13)}$$

where

$$k_{\mathrm{Odiff}} = \nu\,\mathrm{e}^{\frac{-E_{\mathrm{Odiff}}}{T}} \quad \text{(B.14)}$$

$$r_{\mathrm{aLH}} = \mathrm{e}^{\frac{-E_a}{T}} \quad \text{(B.15)}$$

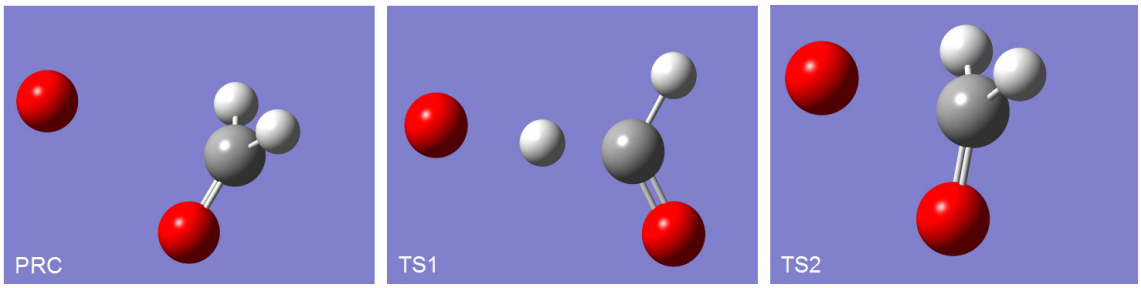

Fig. C.1. Optimized geometries: pre-reactive complex (PRC), Transition State 1 (TS1), and Transition State 2 (TS2), from *the left to the right panels*, respectively.

Table C.1. Calculated activation energies of the O + H_2CO reaction.

		O + H_2CO	PRC[a]	TS1[b]	TS2[c]
M06-2X/cc-pVTZ	Energy (hartree with ZPE[d])	−189.533748	−189.535471	−189.533492	−189.522298
	kJ/mol(with ZPE)	0	−4.5	+0.7	+30.0
	ZPE (kJ/mol)	71.214	73.235	60.578	74.147
	Imaginary frequency	–	–	560i	570i
MP2/cc-pVTZ	Energy (hartree with ZPE)	−189.248868	−189.247962	−189.233923	−189.213331
	kJ/mol(with ZPE)	0	+2.4	+39.3	+93.3
	ZPE (kJ/mol)	70.449	71.788	60.033	76.216
	Imaginary frequency	–	–	2455i	1012i
CCSD(T)/cc-pVTZ	Energy (hartree with ZPE)	−189.307805	–	−189.295737	−189.289862
	kJ/mol(with ZPE at MP2)	0	–	+21.3	+52.9

Notes. [(a)] Pre-Reactive Complex ;[(b)] Transition State 1 ;[(c)] Transition State 2 ;[(d)] Zero Point Energy.

are the thermal diffusion probability of O atoms and the reaction probability of H_2CO+O via LH, respectively. The activation barrier E_a is derived inverting the normalized Arrhenius equation:

$$E_a = -k_b\, T_{\rm eff} \log\,(r_{\rm aER,LH}), \tag{B.16}$$

with either r_{aER} or $r_{\rm aLH}$ according to the mechanism at play. Here

$$T_{\rm eff} = \mu\left(\frac{T_{\rm solid}}{m_{\rm H_2CO}} + \frac{T_{\rm gas}}{m_{\rm O}}\right) = 280 \text{ K for ER, and} \tag{B.17}$$

$$T_{\rm eff} = \mu\left(\frac{T_{\rm solid}}{m_{\rm H_2CO}} + \frac{T_{\rm solid}}{m_{\rm O}}\right) = 55 \text{ K for LH} \tag{B.18}$$

(see Minissale et al. 2013b for more details).

Appendix C: Theoretical calculations

The geometries (Fig. C.1) and energies (Tables C.1 and C.2) were optimized either using DFT with the hybrid meta exchange-correlation functional M06-2X or using classical MP2 method, both methods coupled to the Dunning's correlation (Dunning 1989) consistent polarized valence triple zeta basis set cc-pVTZ. The highly nonlocal M06-2X functional developed by Truhlar et al. (Zhao & Truhlar 2008) is relatively well suited to structures and energetics calculations of the transition states even though this method slightly underestimates barrier energy. We then also calculate the barrier height using full optimized MP2 method, as well as single point CCSD(T) with MP2 geometries in some cases. The unrestricted Hartree-Fock (UHF) formulation has been used since it is a convenient way to describe open-shell and bond-breaking processes. Its use is justified in our study by the fact that we did not observe any significant spin contamination for all the stationary points explored, the quantum average value ⟨S2⟩ of the square of the total spin operator remaining close to 2.00, i.e. the characteristic value for a triplet state. Full geometry optimization was performed throughout. We checked carefully that all the saddle points found are correctly connected to two minima and are characterized by the existence of only one negative eigenvalue of the Hessian matrix corresponding to an imaginary frequency in the normal mode analysis.

Table C.2. Enthalpies of reaction and activation energies calculated at M06-2X/cc-pVTZ level.

Reaction	ΔH_r (kJ/mol)	E_a(kJ/mol)
$^3O + {}^1H_2CO \rightarrow {}^2OH + {}^2HCO$	−60	1.2
$^3O + {}^1H_2CO \rightarrow {}^3OCH_2O$	−80	37
$^3O + {}^1H_2CO \rightarrow CH_2O_2$	+115	>115
$^3OCH_2O \rightarrow {}^3HCOOH$	−23	148
$^3OCH_2O \rightarrow {}^1OCH_2O$	0	Singlet-triplet crossing
$^1OCH_2O \rightarrow {}^1HCOOH$	−438	0
$^2OH + {}^2HCO \rightarrow {}^1HCOOH$	−460	0
$^1HCOOH \rightarrow {}^1H_2O + {}^1CO$	+36	295
$^1HCOOH \rightarrow {}^1CO_2 + {}^1H_2$	−418	293